FIXED POINT ANALYSIS: DYNAMICS OF NON-STATIONARY SPATIOTEMPORAL SIGNALS

A. Hutt

Max Planck-Institute of Cognitive Neuroscience, Stephanstr.1a, 04103 Leipzig, Germany
E-mail: hutt@cns.mpg.de

F. Kruggel

Max Planck-Institute of Cognitive Neuroscience, Stephanstr.1a, 04103 Leipzig, Germany
E-mail: kruggel@cns.mpg.de

A new algorithm for the investigation of unstationary spatiotemporal signals is ontroduced, which consists of two parts: the first determines time windows of non-stationary signal segments and the second aims at low-dimensional dynamical systems describing the detected unstationary behaviour. Results of an application on simulated data, which shows a similar behaviour as a Küppers-Lortz-instability, are discussed.

1 Introduction

The dynamics of spatially extended systems can be measured by sets of multi-detector arrays. The obtained data can be investigated either each channel seperately or as a whole set a signals. Analysis of latter spatiotemporal signals is applied in various different research fields as meteorolgy (e.g. [1]), hydrodynamics (e.g. [2]) or neuroscience [3,4,5,6]. Several methods, which fit multi-dimensional models dynamical models in spatiotemporal signals [7,8,27,9,10] cover the data in full time range. We introduce a method to segments a spatiotemporal signal into parts, which can be described by fixed point dynamics and are modeled by a nonlinear analysis in a further step. This combination is called Fixed Point Analysis.
The segmentation step is introduced as a cluster approach in section 3, where we derive a new cluster criterion by applying the method on the simulated dataset from section 2. In section 4, we introduce a nonlinear analysis method based on perturbation theory and apply it on a simulated Hopf-bifurcation, which contains orthogonal and correlated noise. The combination of both approaches is applied on the dataset of section 2.

2 A simulated dataset: Küppers-Lortz instability

A 144-dimensional simulated dataset is generated by a superposition of 3 spatial modes

$$\mathbf{q}(t) = \sum_{i=1}^{3} A_i(t)\mathbf{v}_i, \tag{1}$$

where the amplitudes $A_i(t)$ determines the temporal behaviour of spatial modes $\mathbf{v}_i$. We choose 3 two-dimensional spatial patterns consisting of 12x12 elements (Fig. 1) and a dynamical system

$$\begin{aligned}
\dot{A}_1 &= \epsilon A_1 - A_1[A_1^2 + (2+b)A_2^2 + (2-b)A_3^2] + \Gamma(t) \\
\dot{A}_2 &= \epsilon A_2 - A_2[A_2^2 + (2+b)A_3^2 + (2-b)A_1^1] + \Gamma(t) \\
\dot{A}_3 &= \epsilon A_3 - A_3[A_3^2 + (2+b)A_1^2 + (2-b)A_2^2] + \Gamma(t)
\end{aligned}$$

to determine the temporal dynamics of the amplitudes. The parameters are set to $\epsilon = 1, b = 2$ and $\Gamma(t) \in [-0.05...0.05]$ represents additive noise, which follows a uniform deviate. This dynamical system arises in a variety of physical systems, where we want to mention the onset of convection in a Rayleigh-Bénard experiment in the presence of rotation. The amplitude equations describe the so-called Kueppers-Lortz instability[11].

Abbildung 1: The basis patterns $\mathbf{v}_1, \mathbf{v}_2$ and $\mathbf{v}_3$.

The differential equation system shows six fixed points

$$\mathbf{A}^0_{\pm 1} = (\pm\sqrt{\epsilon}, 0, 0)^t \quad , \quad \mathbf{A}^0_{\pm 2} = (0, \pm\sqrt{\epsilon}, 0)^t \quad , \quad \mathbf{A}^0_{\pm 3} = (0, 0, \pm\sqrt{\epsilon})^t.$$

As an example, the dynamics near the fixed $\mathbf{A}^0_1$ can be described by

$$\begin{aligned}
\dot{x} &= \epsilon(b-1)x \\
\dot{y} &= -\epsilon(b+1)y \\
\dot{z} &= -2\epsilon z
\end{aligned} \tag{2}$$

with $\mathbf{A} = \mathbf{A}^0_1 + (x, y, z)^t$. For $\epsilon > 0, |b| > 1$, two stable and one unstable local manifold exist. Thus the fixed point represents a saddle point. The fixed points $\mathbf{A}^0_2$ und $\mathbf{A}^0_3$ behave analogously.

A 3-dimensional trajectory is calculated by 2200 integration steps with the initial condition $\mathbf{A}(t=0) = (0.03, 0.2, 0.8)$ and is seen in Fig. 2. The trajectory passes the saddle points $\mathbf{A}_3^0 = (0,0,1)$, $\mathbf{A}_1^0 = (1,0,0)$ and $\mathbf{A}_2^0 = (0,1,0)$ in this sequence, and then returns to $\mathbf{A}_3^0$. By a composition corresponding to Eq. 1, we obtain a spatiotemporal signal (Fig. 3), and one recognizes that these fixed points correspond to the spatial modes $\mathbf{v}_3$, $\mathbf{v}_1$ and $\mathbf{v}_2$.
Now, we aim at extracting the fixed points back from the signal without using any prior knowledge about the internal dynamics, we use the raw signal as input for our method.
In the next section, a clustering approach is introduced and its application on the simulated data is discussed.

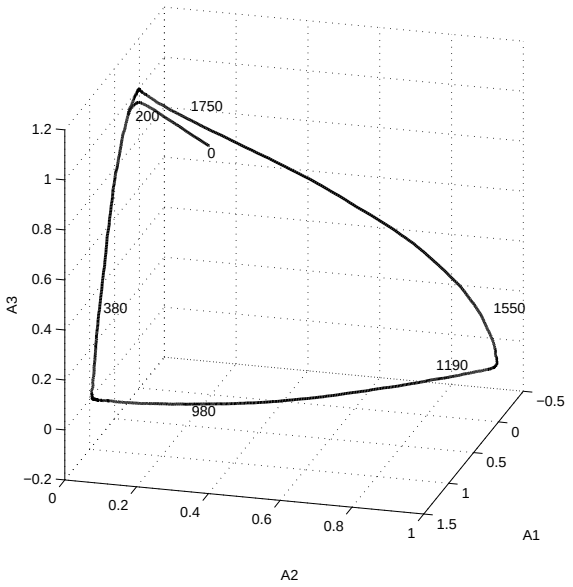

Abbildung 2: Trajectory of the 3-dimensional signal $\mathbf{A}(t)$. It starts near one corner and passes three corners, before it returns to the initial corner. The numbers denote the timesteps of the trajectory at their locations.

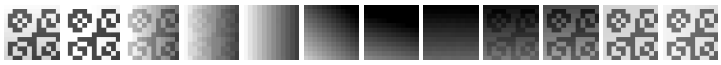

Abbildung 3: Spatiotemporal signal as a temporal sequence of spatial patterns. One recognizes transitions between three basis patterns and a return to the initial pattern.

3 Fixed Point Clustering

We assume a signal trajectory, which shows a sequence of segments governed by saddle point dynamics (Fig. 4). Under the hypothesis, that these segments comprise the main functionality of the underlying system, we aim to extract them from the signal. According to Fig. 4, trajectories approach saddle points along their stable manifolds whereas they leave the vicinity of the fixed points along the unstable manifolds. The signal points accumulate close to the fixed points if the signal is sampled at a constant rate. This accumulation also represents a point cluster in data space. Subsequently, stable manifolds in multi-dimensional signals lead to point clusters (at constant sampling rate) and their detection can be treated as a recognition problem of these clusters in data space [12].
In the present paper we use the K-Means Algorithm (see e.g. [13]) to detect regions in data space with high density of data points. Though there are highly developed and optimized routines [14,15,16] to detect point clusters, we choose one of the simplest methods is probed to be useful here.

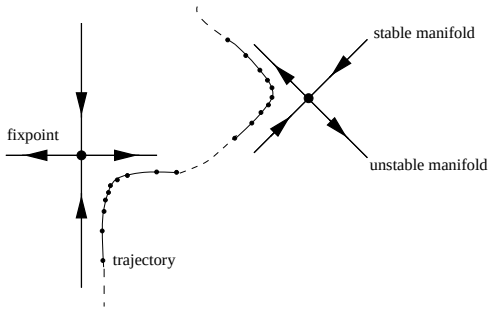

Abbildung 4: Sketch of a trajectory, which passes two fixed points. The transition part is denoted by a dashed line

3.1 The clustering algorithm

A N-dimensional spatiotemporal signal can be described by a data vector $\mathbf{q}(t) \in \Re^N$, where the component $q_j(t_i)$ represents a data point at time i and detection channel j. The clustering algorithm aims at cluster centers $\{\mathbf{k}_k\}$, whose mean Euclidean distance to a set of datapoints $\mathbf{q}(t_i)$ is minimal. The presented implementation follows Moody et. al.[17] and is sketched in Fig. 5. In many clustering algorithms, the number of clusters k is unknown a priorily. We increase k from 2 and analyze each clustering result. This approach leads

to a criterion for valid clusters and is discussed in the next sections.
Cluster centers $\mathbf{k}^0$ are initialized at random locations and their Euclidean distances to each data point are calculated. K-Means defines memberships of data points to a cluster by the smallest Euclidean distance to its center. Thus, data are segmented into k clusters and new cluster centers $\mathbf{k}^1$ are calculated as means of clustered data points. Distances between data points and centers $\mathbf{k}^n$ are re-estimated until a convergence condition is fulfilled. This criterion can be set either as a upper Euclidean distance limit between sequential cluster centers $\mathbf{k}^n, \mathbf{k}^{n+1}$ or or as number of iterations. We choose to limit the number of iterations to 25.

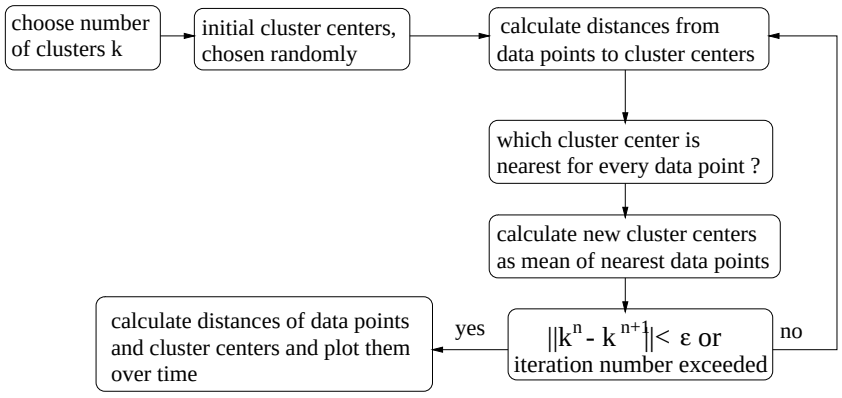

Abbildung 5: The implementation steps of the K-Means algorithm.

3.2 Results of clustering

In a first step, we choose the number of clusters to $k = 3$ and apply the K-Means algorithm on the 144-dimensional simulated dataset. In Fig. 6 , the Euclidean distance from each data point to the determined cluster centers cluster is plotted in respect of the temporal point sequence. When trajectory points are near respectively far from a cluster center, their Euclidean distance to a center is small resp. large. These changes can be observed in Fig. 6 by decreasing and increasing Euclidean distances in time. We consider a data point to be a member of the cluster whose center is closest to the point. The hypothesis, that cluster centers are related to stable manifolds or , in general, fixed points, thus allows an identification of regions of fixed points. The borders of clusters are marked by vertical dashed lines in Fig. 6. A change of 3 states

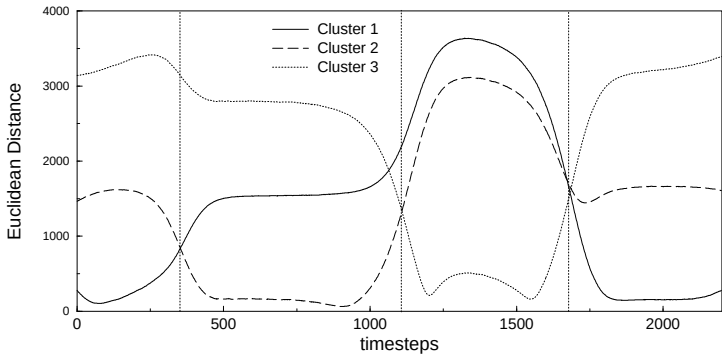

Abbildung 6: Cluster results of the K-Means algorithm with $k = 3$. The plot shows the Euclidean distance of each data point to the detected clusters. Changes of the signal in high-dimensional space between clusters are recognized.

is observed, where the first occuring cluster returns at the end of the signal. Increasing the number of detected clusters k from 2 to 7, we obtain the distance-time plots shown in Fig. 7. The time windows, where the signal has reached the vicinity of a cluster center, remain similar for the investigated clustering results. Since the algorithm has to find k clusters, though there might be only a limited number of clusters $k_d < k$, void clusters are detected at the borders of valid clusters. This leads to first criterion for valid clusters. A cluster can be called valid, if

- its width and location in time remain more or less independent of the number of clusters,
- the Euclidean distance of data points of a cluster to the center is obvious smaller then the Euclidean distance of points to the next nearest cluster center, and the width of the cluster-time window is not too small

Although these criteria are rather heuristic then formal, they proved to be useful in practice[12]. Now, we try to evolve them quantitatively. The first item can be formulated as a sum over all clustering results: valid contributions are additive if they occur for all k, others vanish in the sum as small contributions. Thus the contribution of a valid cluster to the sum has to be large, not reliable clusters should contribute with small values. A good quantity for these contributions is the area between the difference curves of the signal-nearest cluster-distance and signal-next cluster-distance. This definition allows the analytical formulation of the second item and is outlined in Fig. 8. Each data point t_i

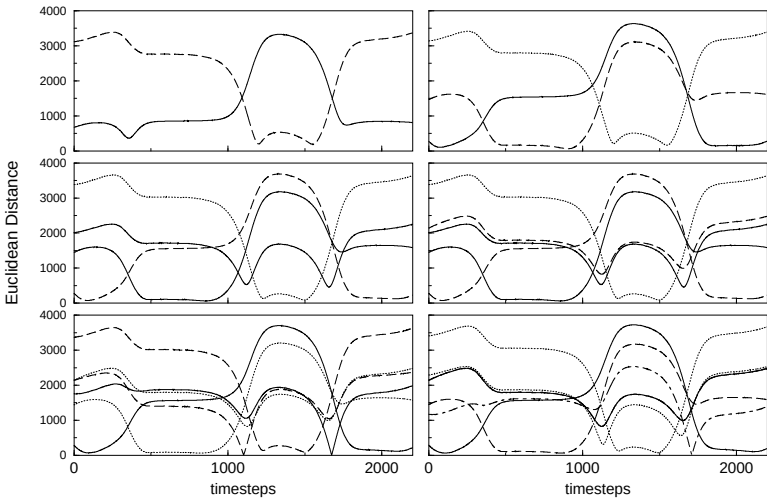

Abbildung 7: Cluster results for $k = 2, .., 7$. The Euclidean distances between data points and detected clusters is shown.

obtains an index corresponding to the cluster j it is member of. The index is equal the relativ area $\frac{A_j^{(k)}(t_i)}{T \sum_j A_j^{(k)}}$, where T is the number of data points. By summing up the indices over K cluster realizations for every data points, we obtain a Cluster Quality Measure (CQM) for every data point:

$$A_r^{(k)}(t_i) = \frac{A_j^{(k)}(t_i)}{\sum_j A_j^{(k)}}$$

$$CQM(t_i) = \frac{\sum_{k=2}^{K \leq T} A_r^{(k)}(t_i)}{\sum_{i=1}^{T} \sum_{k=2}^{K \leq T} A_r^{(k)}(t_i)}.$$

The application on the simulated data with $K = 30$ leads to CQM shown in Fig. 9 and 4 cluster with a high CQM are recognized. Clusters are recognized as plateaus of CQM, its borders are located at rapid changes of CQM.
The original and detected cluster time windows, shown in Fig. 6, 7 and summed up in Fig. 9, are very similar and indicate a correct detection of the fixed points. Now, we aim at modeling the dynamics of the detected trajectory segments by a nonlinear spatiotemporal analysis. If we can obtain reliable models, then the dynamics of the trajectory segments and, consequently, the whole signal is described.

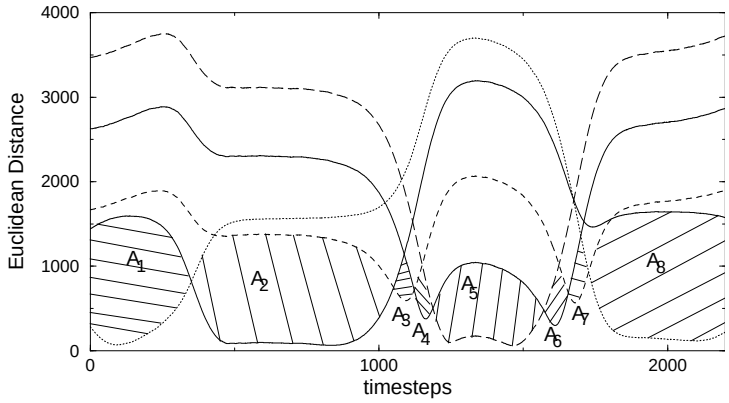

Abbildung 8: Sketch to illustrate the introduced criterion of a clusters validity. The area A_j between two distance curves indexes the data points, which belong to cluster j. Large areas indicates at a high measure of cluster quality.

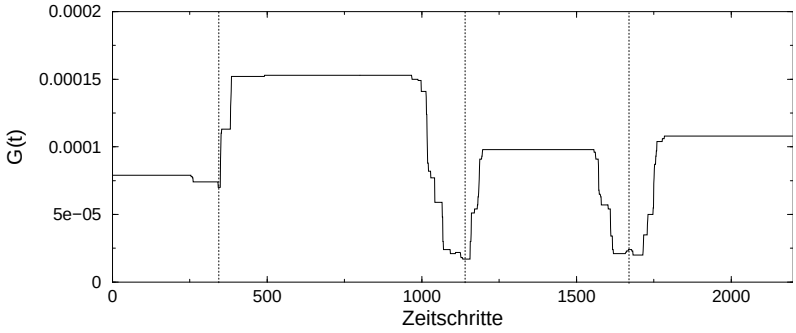

Abbildung 9: The Cluster Quality Measure for every data point. Plateaus denote valid clusters, which are delimited by rapid changes.

4 Spatiotemporal Modelling

In this section, we introduce a nonlinear spatiotemporal analysis [19]. It determines optimal projections of high-dimensional signals onto a low-dimensional basis and fits synchronously a deterministic dynamical system describing the low-dimensional projections.
The presented method is based on Principal Component Analysis (PCA), also known as Karhunen-Loève expansion or Empirical Orthogonal Functions. These methods aim at a few orthonormal spatial modes and projections, which explain most of the variance of a multi-dimensional signal. Extensions in respect of fittings of deterministic dynamical model were proposed by Kirby [20] and Ramsay et. al. [21]. But these methodes leave the basis of modes orthonormal. The orthogonality constraint was first abolished in metereology by Kwasniok [22,23] and in neuroscience by Uhl et.al. [24,25,26]. We outline the latter method in the following.
A spatiotemporal signal $\mathbf{q}(t)$ can be composed by a spatial modes $\mathbf{v}_i$ and amplitudes $x_i(t)$ by

$$\mathbf{q}(t) = \sum_i x_i(t)\mathbf{v}_i \quad , \quad x_i(t) = \mathbf{q}\mathbf{v}_i^\dagger$$

with $\mathbf{v}_i\mathbf{v}_j^\dagger = \delta_{ij}$. The biorthogonal modes $\mathbf{v}_i, \mathbf{v}_j^\dagger$ can be determined by minimizing a costfunction

$$V_s = \frac{< (\mathbf{q} - \sum_i x_i\mathbf{v}_i)^2 >}{< \mathbf{q}^2 >},$$

where $< .. >$ denotes the time average.
A synchronous optimal fit of a dynamical system

$$\begin{aligned} \dot{x}_i(t) &= \Gamma_i^0 + \sum_j \Gamma_{ij}^1 x_j(t) + \sum_j \sum_k \Gamma_{ijk}^2 x_j(t) x_k(t) + \cdots \\ &= f_i[x_j], \end{aligned}$$

which describes the dynamics of the projections $x_i(t)$, can be also obtained by a cost function

$$V_d = \sum_i \frac{< (\dot{x}_i(t) - f_i[x_j])^2 >}{< \dot{x}_i^2 >}.$$

A mutual cost function allows the derivation of spatial modes $\{\mathbf{v}_i\}, \{\mathbf{v}_j^\dagger\}$ and a dynamical system $\mathbf{f}[x_j]$ synchronously

$$V = p \cdot V_1 + (1-p) \cdot V_2 + constraints.$$

The parameter p weights the optimization of spatial modes and dynamical system. Numerical implementation of the method and its applications on epilepsy data [27] and Event-Related-Potential (ERP) data [25] led to new insights in the dynamics of brain signals. But some problems like the influence of the weight factor p to the results and the extensive numerics for high number of spatial modes remain. In order to improve the method, we provide an analytical derivation of optimal spatial modes and a dynamical system.
The new method optimizes a similar cost function

$$V = \sum_i \frac{<(\mathbf{q} - \mathbf{q}\mathbf{w}_i^\dagger \mathbf{w}_i)^2>}{<\mathbf{q}^2>} + \epsilon \cdot \underbrace{\sum_i \frac{<(\dot{y}_i(t) - f_i[y_j])^2>}{<\dot{y}_i^2>}}_{V_d}$$
$$+ \sum_{i,j} \tau_{ij}(\mathbf{w}_i^\dagger \mathbf{w}_j - \delta_{ij}) + \sum_i \alpha_i(\mathbf{w}_i^2 - 1),$$

where τ, α represent Lagrange multipliers of the added constraints and ϵ denotes a weighting factor. Due to the nonlinear differential equation system $\dot{\mathbf{x}} = \mathbf{f}[x_j]$, the variations of V in respect of the biorthogonal basis lead to nonlinear coupled vector equations

$$0 = -2\mathbf{C}\mathbf{w}_k + 2\mathbf{C}\mathbf{w}_k^\dagger + \sum_{j=1}^{N} \tau_{kj}\mathbf{w}_j + \epsilon \frac{\partial V_d}{\partial \mathbf{w}_k^\dagger}$$
$$0 = -2\mathbf{C}\mathbf{w}_k^\dagger + 2(\mathbf{w}_k^\dagger \mathbf{C}\mathbf{w}_k^\dagger)\mathbf{w}_k + \sum_{i=1}^{N} \tau_{ik}\mathbf{w}_i^\dagger + 2\alpha_k \mathbf{w}_k + \epsilon \frac{\partial V_d}{\partial \mathbf{w}_k}.$$

These can be solved by a perturbation expansion in ϵ:

$$\mathbf{w}_k^\dagger = \mathbf{v}_k + \epsilon \mathbf{p}_k^{(1)} + \cdots, \ \tau_{kl} = 0 + \epsilon \tau_{kl}^{(1)} + \cdots$$
$$\mathbf{w}_k = \mathbf{v}_k + \epsilon \mathbf{r}_k^{(1)} + \cdots, \ \alpha_k = 0 + \epsilon \alpha_k^{(1)} + \cdots$$

$$\frac{\partial V_d}{\partial \mathbf{w}_k^\dagger} = \frac{\partial V_d}{\partial \mathbf{w}_k^\dagger}|_0 + \epsilon \frac{\partial V_d}{\partial \mathbf{w}_k^\dagger}|_1 + \cdots, \ \frac{\partial V_d}{\partial \mathbf{w}_k} = \frac{\partial V_d}{\partial \mathbf{w}_k}|_0 + \epsilon \frac{\partial V_d}{\partial \mathbf{w}_k}|_1 + \cdots.$$

Here $\mathbf{v}_i$ denote the orthogonal PCA-modes.[a]
Investigations of the dynamics fit V_d lead to a criterion for an optimal pertur-

[a] It was shown in [19], that the perturbation corrections can be derived analytically for the non-degenerated case, in analogy to Schrödingers perturbation theory in quantum mechanics. It also turns out, that the perturbation theory for non-degenerated PCA-modes with ..... eigenvalues is only valid for low-dimensional deterministic models, whereas the degenerated case should be applied on non-deterministic and thus noisy projections [28].

Abbildung 10: The basis 12x12-patterns $\mathbf{a}_i$ for the multi-dimensional signal.

bation parameter ϵ_c for a minimal V_d. This parameter determines the optimal fit of spatial modes and the dynamical system. Note that $\epsilon = 0$ yields PCA-projections and $\epsilon \neq 0$ new modes and dynamical systems.
As an example, we apply the spatiotemporal analysis on a Hopf-bifurcation with correlated noise, embedded in a 5-dimensional space

$$\mathbf{s}(t) = \sum_{i=1}^{5} u_i(t)\mathbf{a}_i$$

with

$$\begin{aligned} \dot{u}_1 &= \epsilon u_1 - \omega u_2 + (au_1 - bu_2)(u_1^2 + u_2^2) + \Gamma(t) \\ \dot{u}_2 &= \omega u_1 + \epsilon u_2 + (bu_1 + au_2)(u_1^2 + u_2^2) + \Gamma(t) \end{aligned} \tag{3}$$

$$u_j(t) = \sum_{i=1}^{\eta} \rho_i(t) G_i(\mu_i, \sigma_i^2, t) \qquad j = 3, 4, 5.$$

and spatial patterns $\mathbf{a}_i$ (Fig. 10). The correlated noise $\Gamma \in [-2.5; 2.5]$ is equally distributed and the stochastic signal $u_{3,4,5}(t)$ is generated by temporal Gauss functions G_i with equal distributed factors $\rho_i \in [-0.5; 0.5]$, means $\mu_i \in [0; T]$, standard deviations $\sigma_i \in [0; T]$ and $\eta \in [0; T]$, where T denotes the number of timesteps. Since the basis modes $\mathbf{a}_i$ represent 2-dimensional 12x12-patterns, the spatiotemporal signal is 144-dimensional (Fig. 11). Applying the method on the signal, we obtain a best fit of spatial modes and dynamical system for a 2-dimensional model. In Fig. 12, projections of the signal with the first 2

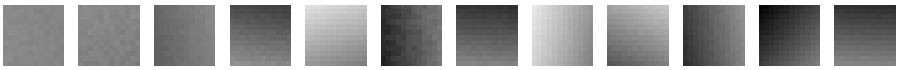

Abbildung 11: Temporal sequence of spatial patterns represent the simulated spatiotemporal signal. Oscillations of the Hopf bifurcation are visible as rotated patterns.

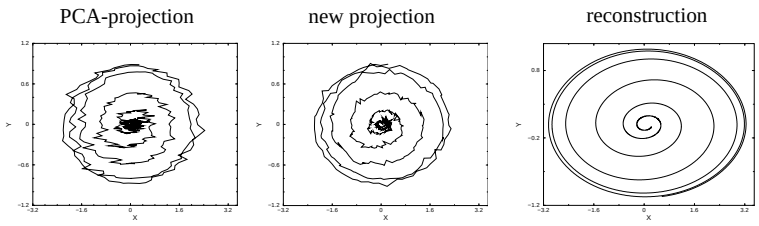

Abbildung 12: Low-dimensional projections of the signal. **Left**: Projections on the first two PCA-modes show a high contribution of noise. **Middle**: Projections on new modes $\mathbf{w}_{1,2}$ show a reduced contribution of noise. **Right**: Reconstructed trajectory from the determined dynamical system. Different scales of the projections and the reconstructed trajectory occur due to scale invariance of least-square fits.

PCA-modes and the perturbation modes are shown. An improvement in respect of the noise contribution to the projections is obvious. The integration of the determined dynamical system is presented in Fig. 12 and the reconstructed signal represents a Hopf-bifurcation described by Eq. 3.
We conclude that the presented method determines an optimal low-dimensional projection in respect of a deterministic dynamical system. Note that this method performs nicely even in case of correlated noise, which is present in most natural systems[29].

5 Fixed Point Analysis (FPA)

In the previous sections, we have addressed the problems of segmenting a spatiotemporal signal into a temporal sequence of spatiotemporal models and the dynamical modeling of its functional parts. A combination of both methods leads to a full functional description of a non-stationary signal.
In the following, we apply FPA on the simulated data of the previous sections. Each of the four detected cluster time windows $T_1 = [30; 230]$, $T_2 = [420; 1010]$, $T_3 = [1200; 1570]$ and $T_4 = [1760; 2200]$ is analyzed by the spatiotemporal method of the previous section. We obtain a good fit for 2-dimensional models in each time window. Figure 13 shows the dynamics fit V_d in respect of the perturbation parameter ϵ, the obtained optimal signal projections and the patterns representing the reconstructed fixed points. The projected trajectories behave analogous to the the equations 2 and the patterns are equivalent to $\mathbf{v}_i$ in Fig. 1 .

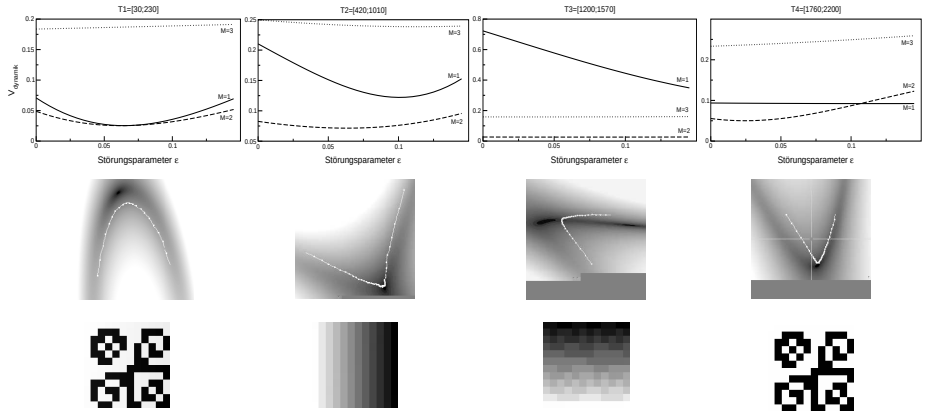

Abbildung 13: Results of the nonlinear analysis method for all detected time windows. **Top**: Plots of $V_d(\epsilon)$ show minima at an optimal perturbation parameter ϵ_c for 2-dimensional models in every time window. **Middle**: optimal projections on two new modes $\mathbf{w}_{1,2}$ for the perturbation parameters ϵ_c. A saddle point dynamics is visible in each time window. **Bottom**: reconstructed patterns, which represent the dynamical fixed points. They accord with the patterns of Section 2.

6 Summary

An algorithm for segmenting a spatiotemporal signal was introduced, where each segment can be described by a fixed point dynamics. A clustering method for high-dimensional signals detects the time windows of the segments. We derived a new criterion for valid clusters, the Cluster Quality Measure CQM. The application on a simulated dataset, which shows non-stationary spatiotemporal behaviour, shows results in good accordance with the signals properties. A nonlinear spatiotemporal analysis completes the Fixed Point Analysis by determining spatiotemporal models for each detected time window. The perturbational approach of the nonlinear analysis allows an analytical derivation of optimal projections and fitted dynamical systems. This guarantees fast numerics, as well for higher dimensional behaviour.
While simulated datasets demonstrate the properties of the algorithm, the investigation of real data is even more interesting. Thus the presented approach has been applied on data from electroencephalography (EEG) and magnetoencephalography (MEG). The measured data show high-dimensional behaviour in space and time and is, of course, far from thermodynamic equilibrium. Nonstationary processes in the brain (i.e. cognitive components) carry functional information about the brain activity. First applications of FPA on Event Re-

lated Potentials(ERP) data [30] revealed relations between clusters and ERP-components. A relevant application of the presented cluster algorithm is given by the automatic detection of ERP-components.

7 Acknowledgments

A. Hutt would like to thank the Max Planck-Institute of Mathematics in the Science in Leipzig, especially Prof. Dr. E. Zeidler, for the financial support of this work.

References

1. G. Plaut, R. Vautard,*Spells of low-frequency oscillations and weather regimes in the northern hemisphere* , J. Atmos. Sc. 51, 210-236 (1994)
2. G. Berkooz, P. Holmes, J. L. Lumley, *The proper orthogonal decomposition in the analysis of turbulent flows*, Ann. Rev. Fluid Mech. 25,539-575 (1993)
3. A. Fuchs, J.A.S. Kelso, H. Haken, *Phase Transitions in Human Brain: Spatial Mode Dynamics*, Int. J. Bifurcation Chaos 2(4), 917-939 (1992)
4. V.K. Jirsa, R. Friedrich, H. Haken, *A Theoretical Model of Phase Transitions in the Human Brain*, Biol. Cybern. 71, 27-35 (1994)
5. H. Haken, *Principles of Brain Functioning. A Synergetics Approach to Brain Activity, Behaviour and Cognition*, Springer, Berlin-Heidelberg-New York (1995)
6. C. Uhl, *Analysis of Neurophysiological Brain Functioning* Springer, Berlin-Heidelberg (1999)
7. C. Uhl, R. Friedrich, H. Haken, *Reconstruction of spatio-temporal signals of complex systems*, Z. Phys. B 92, 211 (1993)
8. C. Uhl, R. Friedrich, H. Haken, *Analysis of spatiotemporal signals of complex systems*, Phys. Rev. E 51(5), 3890-3900 (1995)
9. V.K. Jirsa, H. Haken, *A derivation of a macroscopic field theory of the brain from the quasi-microscopic neural dynamics*, Physica D 99, 503-526 (1997)
10. S. Siegert, R. Friedrich, J. Peinke, *Analysis of data sets of stochastic systems*, Phys. Lett. A 243, pp. 275 (1998)
11. F. H. Busse, K.E. Heikes, *Convection in a Rotating Layer: A Simple Case of Turbulence*, Science **208**, 173 (1980)
12. A. Hutt, M. Svensen, F. Kruggel, R. Friedrich, *Detection of Fixed Points in Spatiotemporal Signals by a Clustering Method*, Phys. Rev. E 61(5), R4691-R4693 (2000)

13. Christoph M. Bishop, *Neural Networks for Pattern Recognition*, Oxford University Press, New York (1995)
14. P. Fränti, J. Kivijärvi, T. Kaukoranta, O. Nevalainen, *Genetic Algorithms for Large-Scale Clustering Problems*, The Computer Journal 40(9), 547-554 (1997)
15. P. Fränti, J. Kivijrvi, *Random swapping technique for improving clustering in unsupervised classification*, 11th Scandinavian Conf. on Image Analysis (SCIA'99), Kangerlussuaq, Greenland, 407-413, vol. 1, 1999.
16. S. Kundu, *Gravitational clustering: a new approach based on the spatial distribution of the points*, Pattern Recognition 32, 1149-1160 (1999)
17. J. Moody, C.J. Darken, *Fast Lerning in Networks of Locally-tuned Processing Units*, Neur. Computation 1(2), 281-294 (1989)
18. I. Borg, J.C. Lingoes, *Multidimensional similarity structure analysis*, Springer, New York (1987)
19. A. Hutt, C. Uhl, R. Friedrich, *Analysis of spatio-temporal signals: A method based on perturbation theory*, Phys. Rev. E 60, 1350 (1999)
20. M. Kirby, *Minimal Dynamical Systems From PDEs Using Sobolev Eigenfunctions*, Physica D 57, pp.466-475 (1992)
21. J.O. Ramsay, B.W. Silverman, *Functional Data Analysis*, Springer, New York (1997)
22. F. Kwasniok, *The Reduction of Complex Dynamical Systems Using Principal Interacting Patterns*, Phsyica D 92, 28-60 (1996)
23. F. Kwasniok, *Optimal Galerkin Approximations of Partial Differential Equations Using Principal Interaction Patterns*, Phys. Rev. E 55(5), 5365-5375 (1997)
24. C. Uhl, R. Friedrich, *Spatio-temporal Analysis of Human Electroencephalograms: Petit-mal Epilepsy*, Physica D 98, 171-182 (1996)
25. C. Uhl, F. Kruggel, B. Opitz, von Cramon D.Y., *A New Concept for EEG/MEG Signal Analysis: Detection of Interacting Spatial Modes*, Human Brain Mapping 6, 137-149 (1998)
26. C. Uhl, R. Friedrich, *Spatio-Temporal Modeling Based on Dynamical Systems Theory*, in *Analysis of Neurophysiological Brain Functioning*, C. Uhl, Springer, Berlin (1999)
27. R. Friedrich, C. Uhl, *Spatio-temporal analysis of human electroencephalograms: Petit-mal epilespy*, Physica D 98, 171-182 (1996)
28. A. Hutt, *Degenerated Perturbation Theory in Spatiotemporal Analysis*, in preperation
29. H. Haken, *Advanced Synergetics*, Springer, Berlin (1993)
30. A. Hutt, F. Kruggel, R. Friedrich, *Dynamische Zustände in raumzeitlichen Signalen, Anwendung auf simulierte Daten und ERP-Datensätze*,

in *Verhandlungen der Deutschen Physikalischen Gesellschaft* VI(35), DY 46.38 (2000)